Evolution Mechanism of Oxide Inclusions in Titanium-Stabilized AISI 443 Stainless Steel

JINGYU LI, GUOGUANG CHENG, QIANG RUAN, JIXIANG PAN, and XINGRUN CHEN

The evolution mechanism of oxide inclusions in Ti-bearing AISI 443 stainless steel was investigated by industrial experiment and thermodynamic calculation. The chemical compositions of steel and the characteristics of inclusions in steel were analyzed. After the addition of Al, the main type of inclusions in molten steel was irregular $MgO{\cdot}Al_2O_3$ spinel. The $MgO{\cdot}Al_2O_3$ inclusions were modified to be spherical $CaO\text{-}Al_2O_3\text{-}MgO$ inclusions after calcium treatment. Thermodynamic calculation results indicated that several ppm Ca could significantly expand the liquid oxide phase field and decrease the stability of spinel. After titanium addition, two types of inclusions were formed: spherical $Al_2O_3\text{-}TiO_x$ inclusions and complex $CaO\text{-}TiO_x\text{-}Al_2O_3\text{-}MgO$ inclusions. The compositions of steel after Ti addition were mostly located in $Al_2O_3\text{-}TiO_x$ stability phase field. Based on the characteristics of inclusions in steel and thermodynamic calculation, inclusions consisting of liquid and $CaTiO_3$ were formed in molten steel with more than 10 ppm Ca during the Ti addition process. The evolution mechanism of oxide inclusions was discussed with the consideration of the initial calcium content before Ti addition.

https://doi.org/10.1007/s11663-018-1331-7

I. INTRODUCTION

TITANIUM has been widely used as an alloy element in stainless steel to suppress chromium carbide precipitation at grain boundary through the formation of more stable titanium carbide, which substantially improves the resistance to intergranular corrosion.[1,2] In addition, the heterogeneous nucleation of delta ferrite on the TiN formed during primary solidification of stainless steel promotes the generation of the equiaxed fine-grained structure.[3] However, the presence of oxide inclusions generally causes serious clogging of submerged entry nozzle (SEN) and surface defects of steel products.[4–7] Thence, it is crucial to predict and control the formation of oxide inclusions in Ti-bearing stainless steel during steelmaking process.

Aluminum is a common final deoxidizer for its high oxygen affinity, which is usually added before the Ti alloy addition to reduce the formation of Ti-containing inclusions and improve Ti yield.[8,9] However, alumina and spinel ($MgO{\cdot}Al_2O_3$) inclusions formed after the Al addition generally lead to the clogging of SEN.[10–12] Many researchers have found that calcium treatment was an effective countermeasure to modify Al_2O_3 or $MgO{\cdot}Al_2O_3$ (MA) inclusions to harmless liquid calcium aluminate inclusions, which could prevent the clogging of SEN during Al-killed steelmaking process.[13–17] Ye *et al.*[13] have described calcium modification of aluminum oxide inclusions using thermodynamic data. They suggested that it is much easier to modify alumina inclusions in a melt with moderate S content at the early treatment stage when temperature is high and particle size is small. The modification of spinel inclusion in liquid steel was investigated by Itoh *et al.*[14] The thermodynamic calculation results indicated that 1 ppm Ca in the steel at 1873 K modified the alumina to the liquid phase and decreased the stability of spinel ($MgO{\cdot}Al_2O_3$) inclusions. Park *et al.*[15] have investigated the inclusion control of ferritic stainless steel by aluminum deoxidation with calcium treatment and concluded that the transformation from alumina to calcium aluminates could be controlled by the diffusion of aluminate polyanions. Yang *et al.*[16] have observed the $MgO\text{-}Al_2O_3\text{-}CaO$ inclusions modified from $MgO{\cdot}Al_2O_3$ spinel inclusions after the calcium treatment. They found that many $MgO\text{-}Al_2O_3\text{-}CaO$ inclusions have a two-layer structure: an outside $CaO\text{-}Al_2O_3$ layer and a $MgO{\cdot}Al_2O_3$ core. It was also found that steel/slag reaction had a great effect on changing the morphology

JINGYU LI and GUOGUANG CHENG are with the State Key Laboratory of Advanced Metallurgy, University of Science and Technology Beijing, Beijing 100083, China. QIANG RUAN, JIXIANG PAN, and XINGRUN CHEN are with the Hongxing Iron & Steel Jiuquan Iron and Steel Co., Ltd., Jiayuguan 735100, Gansu, China. Contact e-mail: chengguoguang@metall.ustb.edu.cn
Manuscript submitted January 20, 2018.
Article published online July 10, 2018.

and composition of alumina and spinel inclusions.[17] Jiang *et al.*[17] have discussed the evolution mechanisms of non-metallic inclusions in molten steel refined by high basicity slag. They found that solid $MgO{\cdot}Al_2O_3$ and MgO inclusions would be inevitably and gradually transformed into CaO-MgO-Al_2O_3 system inclusions with lower melting temperature (< 1773 K) with the increase of Ca content in molten steel due to the reaction of steel and high basicity slag.

The presence of titanium in Al-killed molten steel generally causes more severe clogging of the submerged entry nozzle than Ti-free steel, and the titanium oxide inclusions have been suggested as a possible cause.[5,6,18,19] Thus, many studies of thermodynamic and characteristic of non-metallic inclusions in Al-killed Ti-bearing steel have been carried out.[20–30] Matsuura *et al.*,[20] Jung *et al.*,[22] and Van *et al.*[23] pointed out that Al_2O_3, Ti_2O_3, Ti_3O_5, and Al_2TiO_5 were equilibrium phases of the Al-Ti-O system in molten steel. Wang *et al.*[25–28] found when the Ti/Al ratio in the melt was increased to 15/1 within the Al_2TiO_5 stable phase region, the inclusion population evolved from spherical-dominant ones to irregular ones. Zhang *et al.*[29] reported that irregular titanium aluminates inclusions were generated due to high titanium concentration (nearly 0.5 mass pct) in the melt. As mentioned above, calcium treatment in Al-killed steel has been widely investigated.[13–17] However, only a few available reports have discussed the formation mechanism of oxide inclusions in Al-killed, Ti-bearing stainless steel with Ca treatment.[5,19,30–33] Kruger *et al.*[30] have investigated the effect of calcium treatment on the evolution of spinel ($MgO{\cdot}Al_2O_3$) inclusions in titanium-stabilized AISI 409 stainless steel on an industrial scale. They reported that modification to spherical dual-phase spinel-liquid matrix inclusions was achieved with calcium addition, which eliminated the clogging of SEN for this grade. Kim *et al.*[31] found CaO-SiO_2-Al_2O_3-MgO-TiO_2 inclusions in Al-Ti deoxidized 304 stainless steel. They pointed out that reducing slag basicity (pct CaO/pct SiO_2) was the most effective way to avoid the harmful inclusions with $CaO{\cdot}TiO_2$ crystallized phase. The effect of Ca and Ti addition sequence on the inclusion behavior in Al-killed stainless steel have been investigated by Seo *et al.*[32] The experimental results indicated that conducting Ca treatment prior to Ti alloying could reduce the formation of spinel inclusions. Zheng *et al.*[5] investigated the clogging of SEN of Ti-bearing 321 stainless steel with Ca treatment, and found two types deposition, namely TiN and $CaO{\cdot}TiO_2$. Qian *et al.*[19] also found that the $CaO{\cdot}TiO_2$-rich ($CaO{\cdot}TiO_2$-$MgO{\cdot}Al_2O_3$) complex inclusions in Ti-bearing stainless steel were mainly inclusions in the clogging of SEN. What is more, the effect of calcium content on the formation of oxide inclusions in titanium-stabilized AISI 443 stainless steel has never been specifically studied yet.

In current work, to reveal the evolution mechanism of oxide inclusions in Ti-bearing 20Cr stainless steel, steel samples were taken at different stages in industrial trial. The characteristics of inclusions in steel samples were determined by scanning electron microscopy and energy-dispersive X-ray spectroscopy (SEM + EDX). The formation mechanism and phase stability of inclusions observed in steel were investigated with the aid of thermodynamic calculation. At the same time, the effect of the initial calcium content before Ti addition on the evolution of oxide inclusions was discussed through the coupling of thermodynamics calculation and experimental results.

II. METHODOLOGY

A. *Experimental Procedures*

The characteristics of inclusions in industrially produced AISI 443 stainless steel were investigated. The steelmaking process of titanium-bearing stainless steel was "100 ton electric arc furnace (EAF) → 100 ton argon oxygen decarburization furnace (AOD) → 100 ton vacuum oxygen decarburization (VOD) → 100 ton ladle furnace (LF) → continuous casting (CC)," as shown in Figure 1. Scrap and alloy were melted in the EAF, and then the molten steel was subsequently decarburized, deoxidized, and desulfurized in AOD. Before tapping into the ladle, most of the slag was removed. The ladle refractory was made by MgO-chromite bricks. After the additional decarburization and degassing in the VOD, ferrosilicon was added to deoxidize. During LF refining process, aluminum was added first for additional deoxidation. Then, titanium wire was added after calcium treatment in LF. When the chemistry and temperature were on specification, the heat was transported to the continuous casting platform.

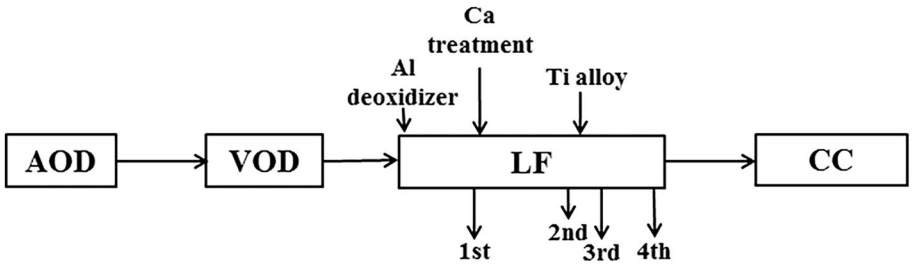

Fig. 1—Schematic illustration of sampling locations.

Table I. Chemical Compositions of Steel Samples in Three Heats (Mass Percent)

Heat No.	Sample No.	Ti	Al	Ca	Mg	O
A	A1	0.0009	0.016	0.0011	0.0006	0.0074
	A2	0.0017	0.016	0.0016	0.0005	0.007
	A3	0.3	0.017	0.0007	0.0004	0.0066
	A4	0.27	0.016	0.0004	0.0004	0.0066
B	B1	0.0014	0.0045	0.0013	0.0008	0.0086
	B2	0.0023	0.0076	0.0023	0.0008	0.0067
	B3	0.21	0.012	0.0012	0.0007	0.0035
	B4	0.18	0.012	0.0002	0.0005	0.0050
C	C1	0.002	0.013	0.0011	0.0006	0.0046
	C2	0.0012	0.012	0.0007	0.0006	0.0037
	C3	0.2	0.017	0.0005	0.0005	0.0035
	C4	0.17	0.012	0.0002	0.0006	0.0033

Three heats of experiments were totally carried out. Steel samples were taken before the addition of Ca, before feeding titanium wire, at 10 minutes after the addition of Ti, and at the end of LF refining, respectively. The lollipop steel samples taken in the steelmaking process were immediately quenched in water. Schematic illustration of sampling locations is shown in Figure 1.

B. *Composition Analysis and Inclusion Characterization*

Obtained steel samples were prepared for chemical analysis and inclusion observation. The total oxygen contents were analyzed by the inert gas fusion-infrared absorptiometry method with an accuracy of ± 1 ppm. The acid-soluble Al, Ca, and Mg contents in steel were determined by the inductively coupled plasma optical emission spectrometry method (ICP-OES) with ± 5 pct relative standard deviation. The alloying element contents in steel were measured by the alkali fusion acid dissolution method. The chemical compositions of steel specimens are shown in Table I. The morphologies and compositions of non-metallic inclusions on the mirror-polished surfaces of the steel specimens were analyzed with the aid of an automatic scanning electron microscope (EVO18-INCAsteel, ZEISS Co., Ltd.), combined scanning electron microscopy (SEM) with energy-dispersive X-ray spectroscopy (EDS). The maximum diameter of the inclusion was defined as the size of the inclusion. For the accuracy of automated EDS analysis of inclusions, the size was taken larger than 1 μm, because the interaction volume may spread into the steel and excite electrons from the surrounding environment of the inclusions with diameters smaller than 1 μm.[34–37]

III. RESULTS AND DISCUSSION

A. *Characterization of Inclusions*

After the addition of Al in LF, the main inclusions were $MgO{\cdot}Al_2O_3$ (MA), as shown in Figure 2(a). At the same time, a few Al_2O_3 and $MgO\text{-}Al_2O_3\text{-}CaO$ was also observed. According to the irregular shape of the inclusions, it is clear that they were solid at steelmaking temperatures. Elemental mapping of a typical $MgO{\cdot}Al_2O_3$ inclusion is shown in Figure 3(a). The compositions of Al, Mg, and O in the square inclusion were homogeneous. The MgO-based refractory supplied soluble Mg in molten steel to form MgO in inclusions.[33,38,39]

After the calcium treatment, the typical type of inclusions was spherical $CaO\text{-}Al_2O_3\text{-}MgO$, as shown in Figure 2(b). Elemental mapping of a typical $CaO\text{-}Al_2O_3\text{-}MgO$ inclusion is shown in Figure 3(b). This inclusion consisted of a spinel crystal embedded in a $CaO\text{-}Al_2O_3$ liquid matrix. The non-uniform distribution of the inclusions was related to the difference of modification ability of $MgO{\cdot}Al_2O_3$ spinel and alumina with calcium treatment. It has been reported that the modification of spinel with calcium was less effective than the modification of pure alumina.[5,40–42]

After the addition of Ti-cored wire, two typical inclusion types were found: homogeneous small size $Al_2O_3\text{-}TiO_x$ inclusions (Figure 2(c1)) and complex large size $CaO\text{-}TiO_x\text{-}Al_2O_3\text{-}MgO$ inclusions (Figures 2(c2) and (c3)). The morphologies of inclusions were different, including irregular shape and spherical shape. Figure 3(c) shows an elemental mapping of a multilayer inclusion. As can be seen, the inclusion could be divided into two layers: the inner layer was an irregular shape $MgO{\cdot}Al_2O_3$ core, and the main compositions of the outer layer were $CaO\text{-}Al_2O_3\text{-}TiO_x$.

At the end of LF, the types of inclusions were essentially the same as those after titanium addition, as shown in Figure 2(d). With the agitation of argon gas in liquid steel, the inclusions gradually polymerized and floated up, which led to the decrease of total oxygen content during LF refining process.[34] A polymerized inclusion was observed in steel specimen taken at the end of LF, as shown in Figure 2(d3). Figure 3(d) shows an elemental mapping of a dual-phase inclusion, with a $MgO{\cdot}Al_2O_3$ spinel core and a $CaO\text{-}Al_2O_3\text{-}TiO_x$ outer layer. The size of the inner core of inclusions in sample 4 was usually smaller than that of sample 3, which might be due to the ongoing reaction between molten steel and inclusions after the addition of titanium.

To investigate the evolution of inclusions, the compositions of inclusions in steel samples were projected onto the 1873 K isotherm of CaO-MgO-Al_2O_3 ternary system phase diagrams, as shown in Figure 4. The phase diagram and liquid oxide phase field (red outlined area) of the CaO-MgO-Al_2O_3 ternary system at 1873 K were marked with the aid of FactSage™ 7.0 software. In the CaO-Al_2O_3-MgO phase diagram, there was an all liquid area with the CaO content ranging from 27 to 57 wt pct. This indicated that reasonably increasing the CaO content in $MgO{\cdot}Al_2O_3$ inclusions could make the composition of inclusions in the liquid area. After the addition of aluminum, the main compositions of inclusions concentrated in or around the spinel ($MgO{\cdot}Al_2O_3$) region with a small amount of CaO. The MgO contents of inclusions in sample B1 were slightly higher than those of samples A1 and C1, which might be due to the high Mg content and low Al content in sample B1. After calcium treatment, the CaO contents of most inclusions in sample A2 and sample B2 have increased. Meanwhile, the CaO content of inclusions in sample C2 containing lower Ca content increased less. It can be seen that the inclusion compositions were close to the liquid oxide phase field. After the addition of titanium, the Al_2O_3

Fig. 3—Elemental mapping of typical inclusions at each stage: (*a*) ▶ $MgO{\cdot}Al_2O_3$ inclusion after Al addition. (*b*) Multilayer CaO-MgO-Al_2O_3 inclusion after calcium treatment. (*c*) Multilayer CaO-MgO-Al_2O_3-TiO_x inclusion 10 min after Ti addition in LF. (*d*) Multilayer CaO-MgO-Al_2O_3-TiO_x inclusion at LF end.

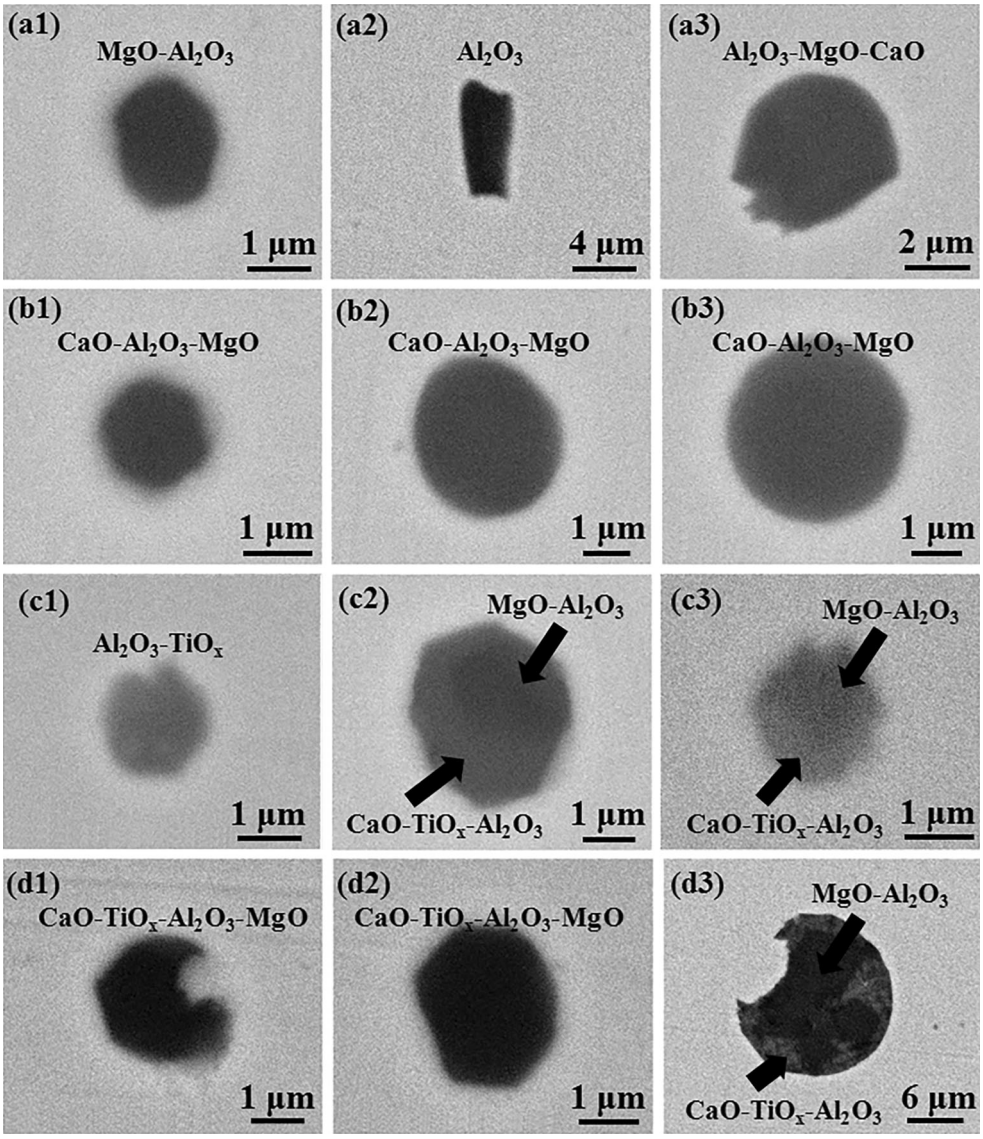

Fig. 2—Morphology and composition of typical inclusions encountered in samples: (*a1*) irregular $MgO{\cdot}Al_2O_3$ inclusion, (*a2*) irregular Al_2O_3 inclusion, (*a3*) spherical Al_2O_3-MgO-CaO inclusion after Al addition. (*b1*) Spherical CaO-Al_2O_3-MgO inclusion, (*b2*) spherical CaO-Al_2O_3-MgO inclusion, (*b3*) spherical CaO-Al_2O_3-MgO inclusion after calcium treatment. (*c1*) Spherical Al_2O_3-TiO_x inclusion, (*c2*) irregular CaO-MgO-Al_2O_3-TiO_x inclusion, (*c3*) irregular CaO-MgO-Al_2O_3-TiO_x inclusion 10 min after Ti addition. (*d1*) Complex CaO-TiO_x-Al_2O_3-MgO inclusion, (*d2*) complex CaO-TiO_x-Al_2O_3-MgO inclusion, (*d3*) complex CaO-TiO_x-Al_2O_3-MgO inclusion at LF end.

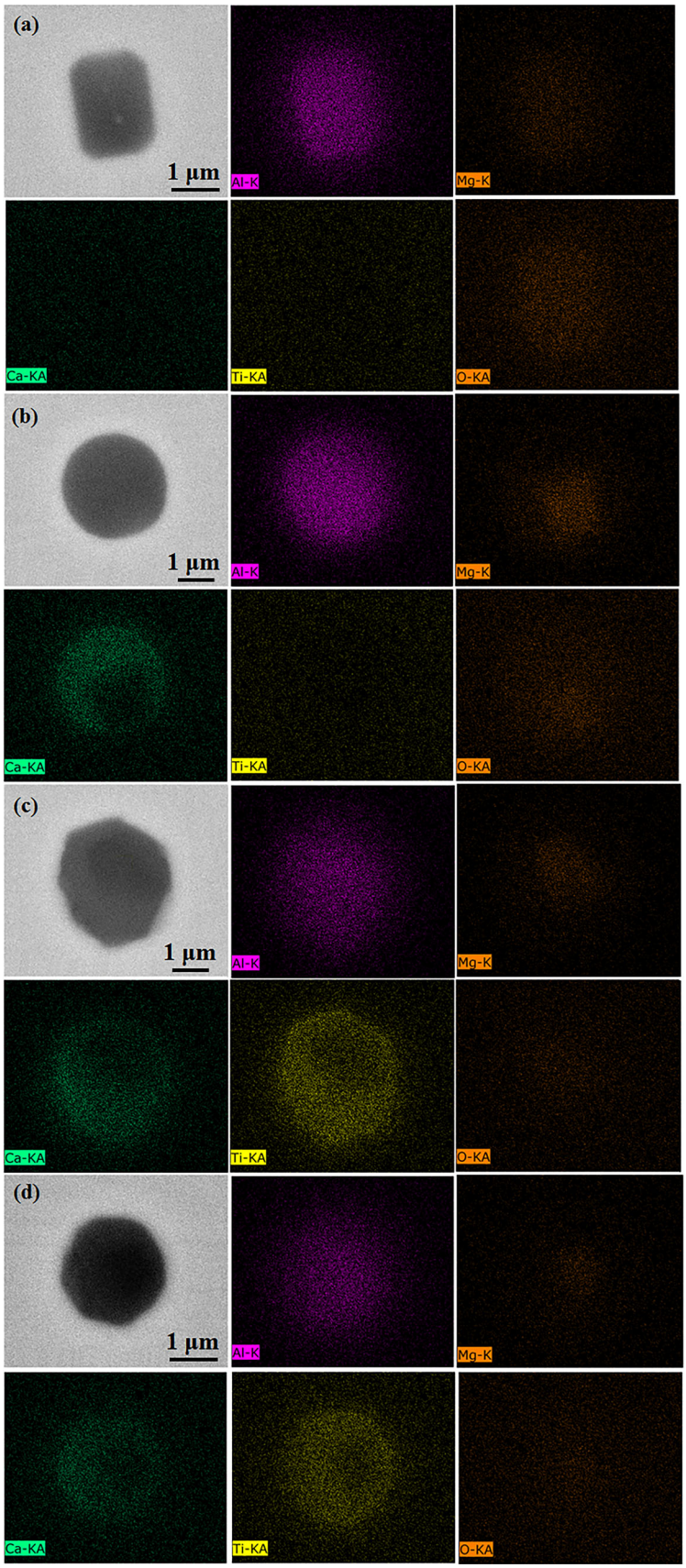
(a)
1 μm
Al-K
Mg-K
Ca-KA
Ti-KA
O-KA
(b)
1 μm
Al-K
Mg-K
Ca-KA
Ti-KA
O-KA
(c)
1 μm
Al-K
Mg-K
Ca-KA
Ti-KA
O-KA
(d)
1 μm
Al-K
Mg-K
Ca-KA
Ti-KA
O-KA

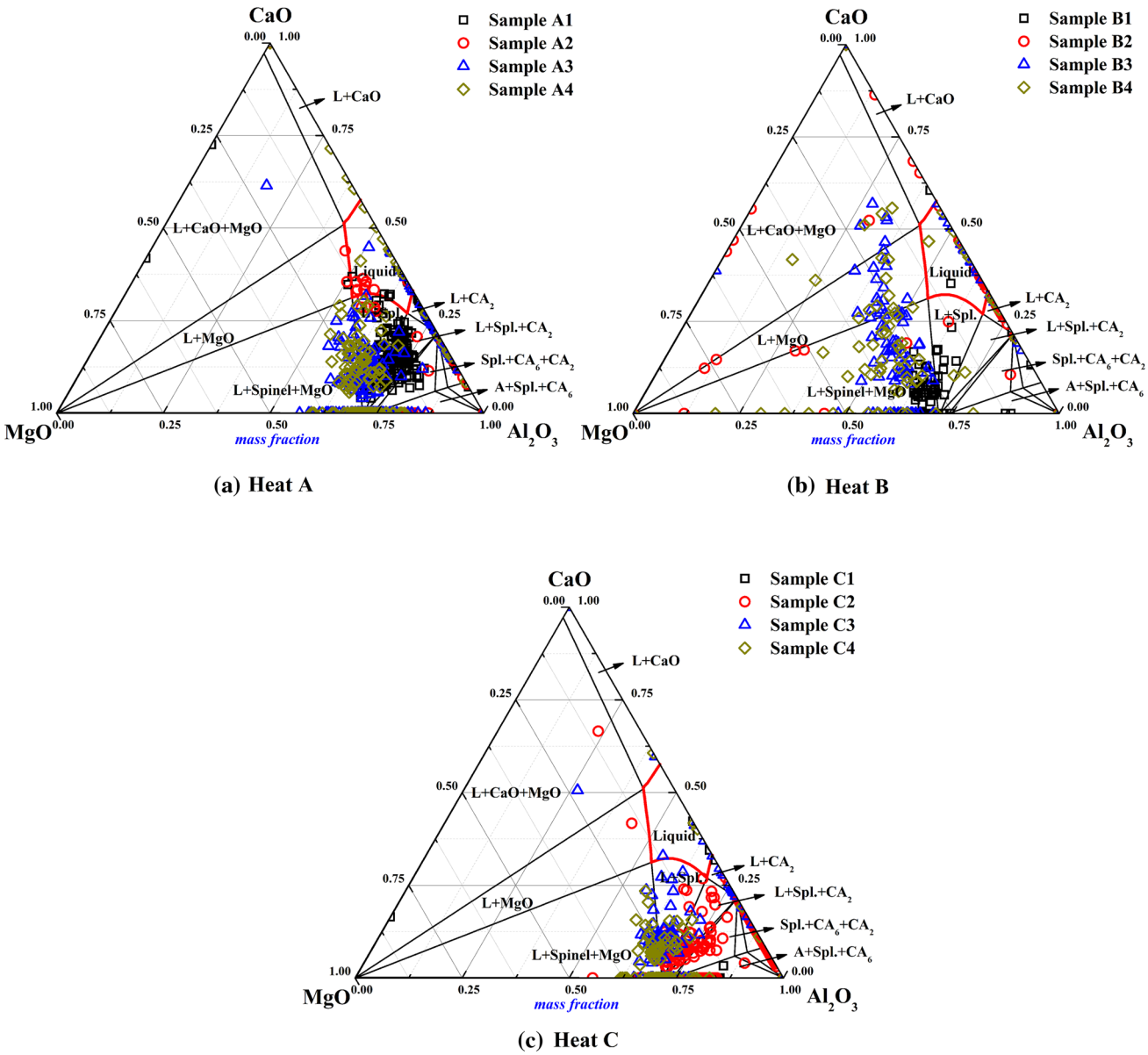

Fig. 4—Compositions of inclusions in steel samples, projected onto the 1873 K isotherm of the CaO-Al_2O_3-MgO ternary diagram: (*a*) compositions of inclusions in heat A. (*b*) Compositions of inclusions in heat B. (*c*) Compositions of inclusions in heat C. (Liquid (L): Liquid oxide, CA_2: $CaO{\cdot}2Al_2O_3$, CA_6: $CaO{\cdot}6Al_2O_3$, Spinel (Spl.): $MgO{\cdot}Al_2O_3$, A: Al_2O_3).

contents of inclusions decreased slightly. Owing to higher Ca content in sample B3, the CaO contents of inclusions in sample B3 were higher than that of sample A3 and sample C3. At the end of LF refining, the composition distribution of inclusions has not changed much in CaO-MgO-Al_2O_3 ternary system.

The oxidation state of titanium in molten steel was determined from the titanium content in steel and the oxygen partial pressure, such as TiO, TiO_2, Ti_3O_5, Ti_2O_3, and Ti_4O_7.[9,43] According to the previous research, the stable deoxidized product was Ti_3O_5 in the present work.[9,43,44] The mass percentages of CaO, Al_2O_3, and Ti_3O_5 of inclusions were plotted on the CaO-Al_2O_3-Ti_3O_5 ternary compositional diagram, as shown in Figure 5. The phase diagram and liquid oxide phase field (red outlined area) of the CaO-Al_2O_3-Ti_3O_5 system under the oxygen partial pressure of $P_{O_2} = 10^{-12}$ atm were calculated by FactSage™ 7.0 software. After the addition of titanium, there were a lot of newly formed complex Ti-containing inclusions, as shown in Figure 5. Some inclusions in sample A3 contained high Ti_3O_5 concentrations due to the high Ti content in molten steel. In addition, some inclusions in sample A3 were located in or close to the perovskite region. There were a lot of inclusions located in the all liquid oxide phase field, (liquid + $CaTiO_3$ + $CaO{\cdot}2Al_2O_3$) phase field, and (liquid + $CaTiO_3$) phase region in sample B3, which might be due to the high calcium content. Many inclusions in sample C3 were located in the all liquid phase field and (liquid + Al_2O_3) phase field. At the end of LF, the number of inclusions containing high Ti_3O_5 in sample A4 decreased. However, there still

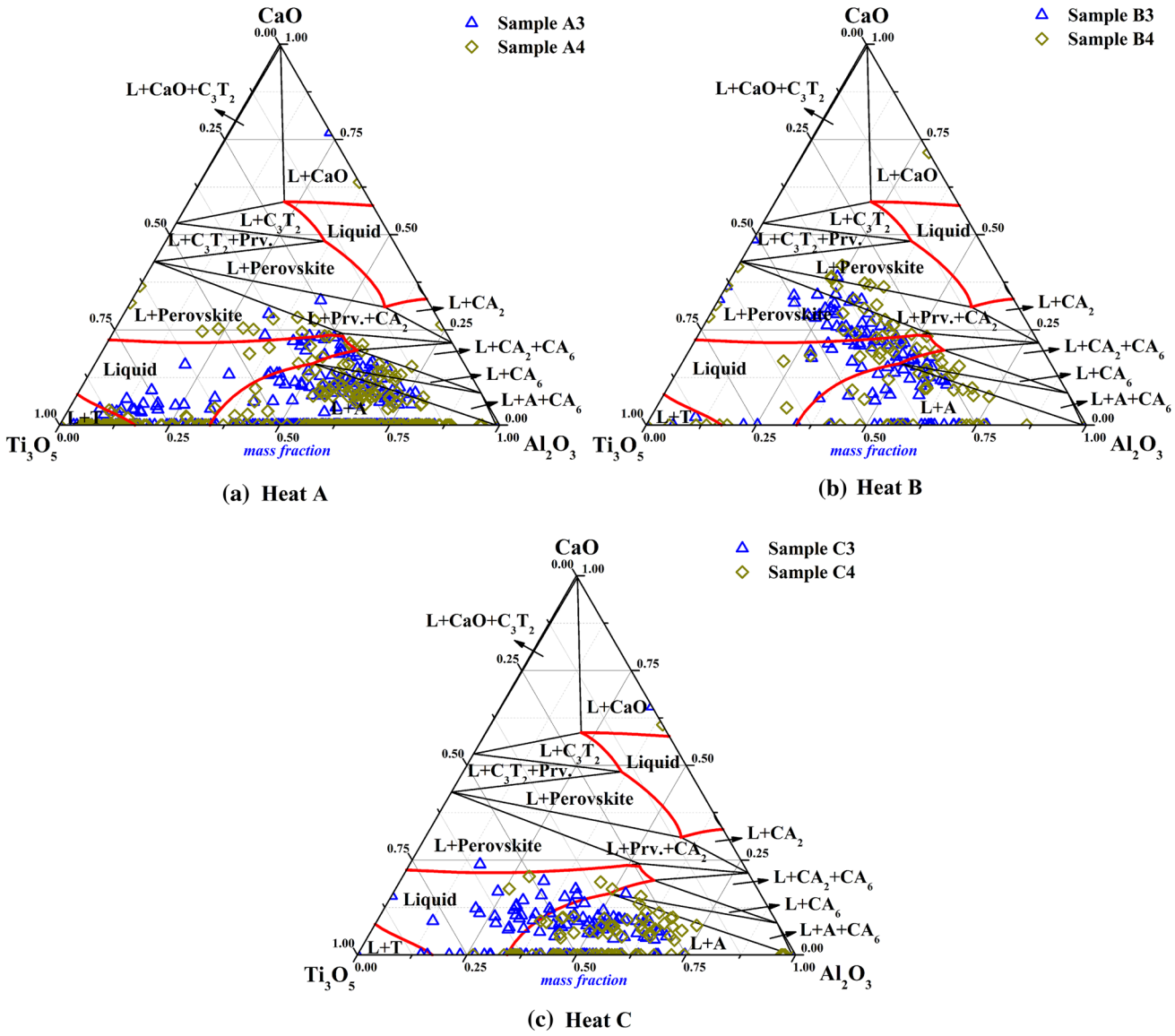

Fig. 5—Composition distributions of inclusions in $CaO-Al_2O_3-Ti_3O_5$ phase diagrams. Solid lines represent the boundary line of different phases at 1873 K under the oxygen partial pressure of $P_{O_2} = 10^{-12}$ atm: (*a*) compositions of inclusions in heat A. (*b*) Compositions of inclusions in heat B. (*c*) Compositions of inclusions in heat C. (Liquid (L): Liquid oxide, CA_2: $CaO{\cdot}2Al_2O_3$, CA_6: $CaO{\cdot}6Al_2O_3$, A: Al_2O_3, perovskite (Prv.): $CaTiO_3$, C_3T_2: $3CaO{\cdot}2TiO_2$, T: Ti_3O_5).

existed some inclusions located in the (liquid + perovskite) phase field. Just same as the composition distribution of sample B3, many inclusions in sample B4 were still located in the phase fields that contain perovskite or $CaO{\cdot}2Al_2O_3$. Comparing to sample C3, the number of liquid oxide inclusions in sample C4 decreased.

B. *Thermodynamic Calculation of Inclusion Formation*

Spinel and alumina inclusions could lead to the clogging of SEN,[4,6,10,45,46] which were also observed in the present experiment. Thus, the phase stability diagram of Al-Mg-O system in Fe-20Cr steel at 1873 K was calculated with the aid of FactSage™ 7.0 software to investigate the formation mechanism of these inclusions. It can be seen from the phase diagram in Figure 6 that alumina, spinel ($MgO{\cdot}Al_2O_3$), and MgO are mainly phases in molten steel with magnesium and aluminum contents ranging from 0.1 to 100 ppm and 1 ppm to 1 wt pct, respectively. The boundary lines of each phase field were evaluated using [O] ppm as a parameter. The compositions of steel samples are marked in Figure 6. As can be seen, these compositions were located in spinel area. The main inclusions in samples taken after aluminum addition were spinel inclusions. However, some alumina inclusions were also observed, which might be formed in a non-equilibrium state after the

addition of Al. Many researchers found that calcium treatment could effectively modify spinel or alumina inclusions to harmless liquid inclusions, which could prevent the clogging of SEN.[13–17,39] Thus, the stability diagrams of Mg-Al-O phase with 1 ppm and 5 ppm Ca contents in Fe-20Cr steel at 1873 K were calculated, as shown in Figure 7. As can be seen in Figure 7, there are three oxide fields, *viz*. all liquid oxide, spinel ($MgO{\cdot}Al_2O_3$), and MgO. After the addition of 1 ppm Ca, the spinel phase field shrunk and the Al_2O_3 phase field disappeared, while the all liquid oxide phase field appeared. The spinel stability phase field almost disappeared when a Fe-20Cr steel with 5 ppm calcium was present. It can be concluded that several ppm Ca can significantly expand the all liquid oxide phase field and decrease the size of the stability field of spinel. However, the MgO phase field remained present with the addition of 1 to 5 ppm Ca. The experimental results are marked in Figure 7. Although the inclusion compositions were located in the spinel phase field for a Fe-20Cr steel with 1 ppm Ca, most of the compositions were located in the all liquid oxide phase field when the Fe-20Cr steel contained 5 ppm Ca. According to the phase diagrams in Figures 6 and 7, calcium treatment is an effective way to modify alumina and spinel inclusions to all liquid oxide inclusions. What is more, Todoroki *et al*.[45] have prevented nozzle clogging in an industrial experiment by controlling the inclusion composition in the MgO phase field instead of the spinel or alumina phase fields. As shown in Figures 6 and 7, increasing the Mg content to more than 10 ppm could promote the formation of MgO and reduce the formation of spinel and alumina, which might prevent the clogging of SEN.

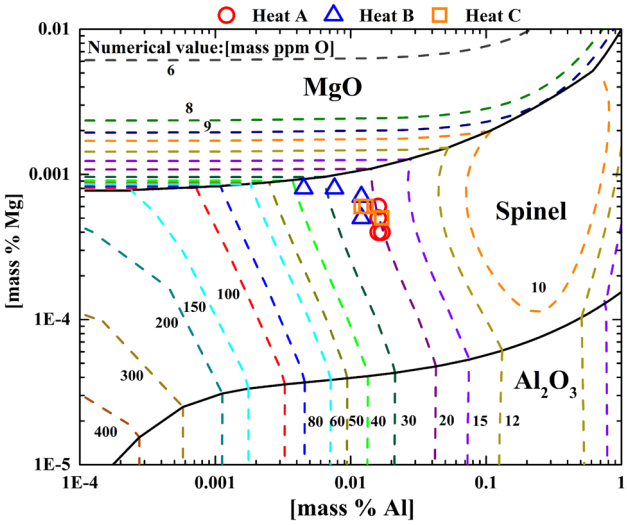

Fig. 6—Calculated oxide stability diagram of Al-Mg-O system with iso-oxygen contours (in ppm) in Fe-20Cr steel at 1873 K.

After the addition of titanium, inclusions containing titanium oxides were observed in certain of the samples. The proper aluminum content before the Ti addition is crucial for controlling the formation of oxide inclusions and getting high titanium yield. Thus, the phase stability diagram of Al-Ti-O system in Fe-20Cr steel at 1873 K was calculated with the aid of FactSage™ 7.0 software, as shown in Figure 8. There are four oxide fields, *viz*. Al_2O_3, Ti_2O_3, Ti_3O_5, and liquid oxide, with the content range of Ti from 0.001 to 1 wt pct and Al from 1 ppm to 1 wt pct. The Ti_2O_3 phase is stable when the titanium content ranges from 0.3 to 1 wt pct, while the Ti_3O_5 phase is stable when the titanium content is less than 0.3 wt pct. The phase boundary between Ti_3O_5 phase field and Ti_2O_3 phase field is 0.3 wt pct titanium content in Fe-20Cr molten steel at 1873 K. What is more, too many alumina inclusions would be formed when the composition of steel containing high Al content was located in Al_2O_3 phase field. Similarly, titanium would

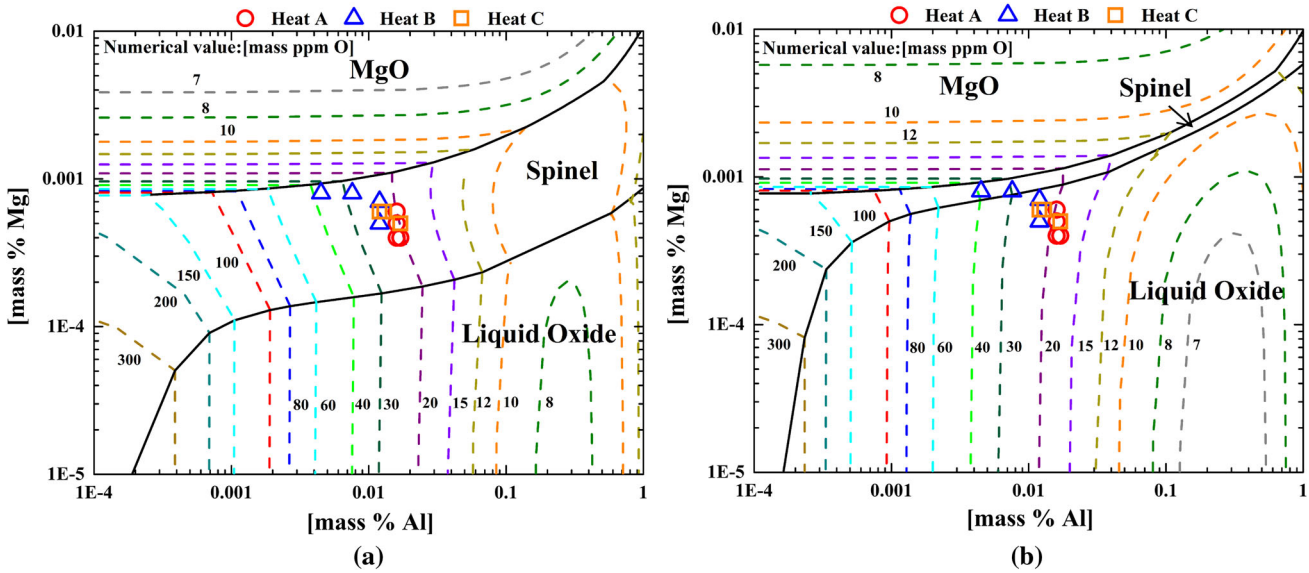

Fig. 7—Calculated oxide stability diagrams of Al-Mg-O system with iso-oxygen contours (in ppm) in (*a*) Fe-20Cr-1 ppm Ca steel and (*b*) Fe-20Cr-5 ppm Ca steel at 1873 K.

be oxidized when the composition of steel containing low Al content was located in titanium oxide phase field (Ti_2O_3 phase field or Ti_3O_5 phase field). Hence, the appropriate Al content and Ti content in molten steel should be located in the all liquid phase field, which would help to reduce the formation of oxide inclusions and increase the titanium yield. The compositions of steel samples taken after the titanium addition are marked in Figure 8. It can be seen that most of the compositions were located in or close to the liquid oxide phase field, which was good for controlling the formation of inclusions. At the same time, researchers have argued about the existence of liquid Al_2O_3-TiO_x phase. Some researchers[20,23] insisted that only Al_2O_3, Ti_2O_3, Ti_3O_5, and Al_2O_3-Ti_3O_5 were stable phases. However, Jung *et al.*[22] and Ruby *et al.*[47] reported that there was a liquid phase between Al_2O_3 and Ti_3O_5 phase. Wang *et al.*[26] also found spherical Al-Ti-O inclusions in steel with the Ti/Al ratio smaller than 15/1. In the present experiment, liquid Al_2O_3-TiO_x inclusions were observed in sample C3, as shown in Figure 9. The compositions of Al, Ti, and O in the spherical inclusion were homogeneous. Based on the shape and composition of this inclusion, it indicated that it was a liquid Al_2O_3-TiO_x inclusion at steelmaking temperature.

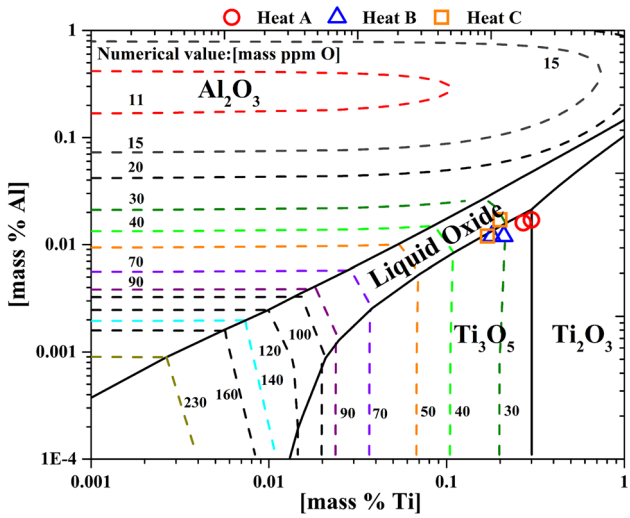

Fig. 8—Calculated oxide stability diagram of Al-Ti-O system with iso-oxygen contours (in ppm) in Fe-20Cr steel at 1873 K (liquid oxide: Al_2O_3-TiO_x).

The effect of initial calcium content in molten steel on the formation of inclusions during titanium addition process has not been discussed. Therefore, the evolution of inclusions with different calcium contents in Fe-20Cr steel containing 150 ppm Al and 50 ppm O with the increase of titanium content was calculated with the aid of FactSage™ 7.0 software, as shown in Figure 10. When the calcium content in steel was 1 ppm, the transformed sequence of oxide inclusions was $CaO{\cdot}6Al_2O_3$ (CA_6), Al_2O_3, liquid oxide phase, and TiO_x with the Ti content ranging from 0 to 0.5 mass pct. The CA_6 and Al_2O_3 phase fields disappeared and $CaO{\cdot}2Al_2O_3$ (CA_2) phase field formed in the molten steel containing 5 ppm Ca. After the calcium content increased to 10 ppm in the steel, the solid perovskite phase (CT) was formed with the titanium content ranging from 0.01 to 0.07 mass pct. In the molten steel containing 15 ppm Ca, the concentration of CT inclusions increased as the Ti concentration increased up to 0.03 mass pct. In addition, the content range of titanium in steel containing CT phase increased from 0.01 to 0.18 mass pct. The titanium contents of steel samples

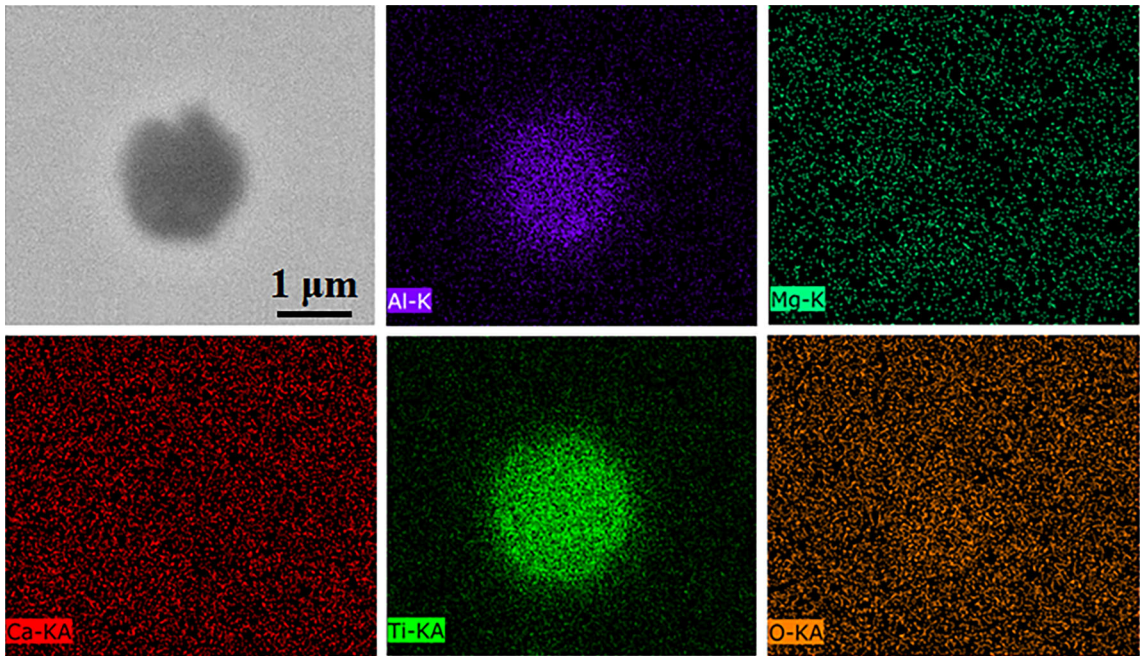

Fig. 9—Elemental mapping of a typical Al_2O_3-TiO_x inclusion in sample C3.

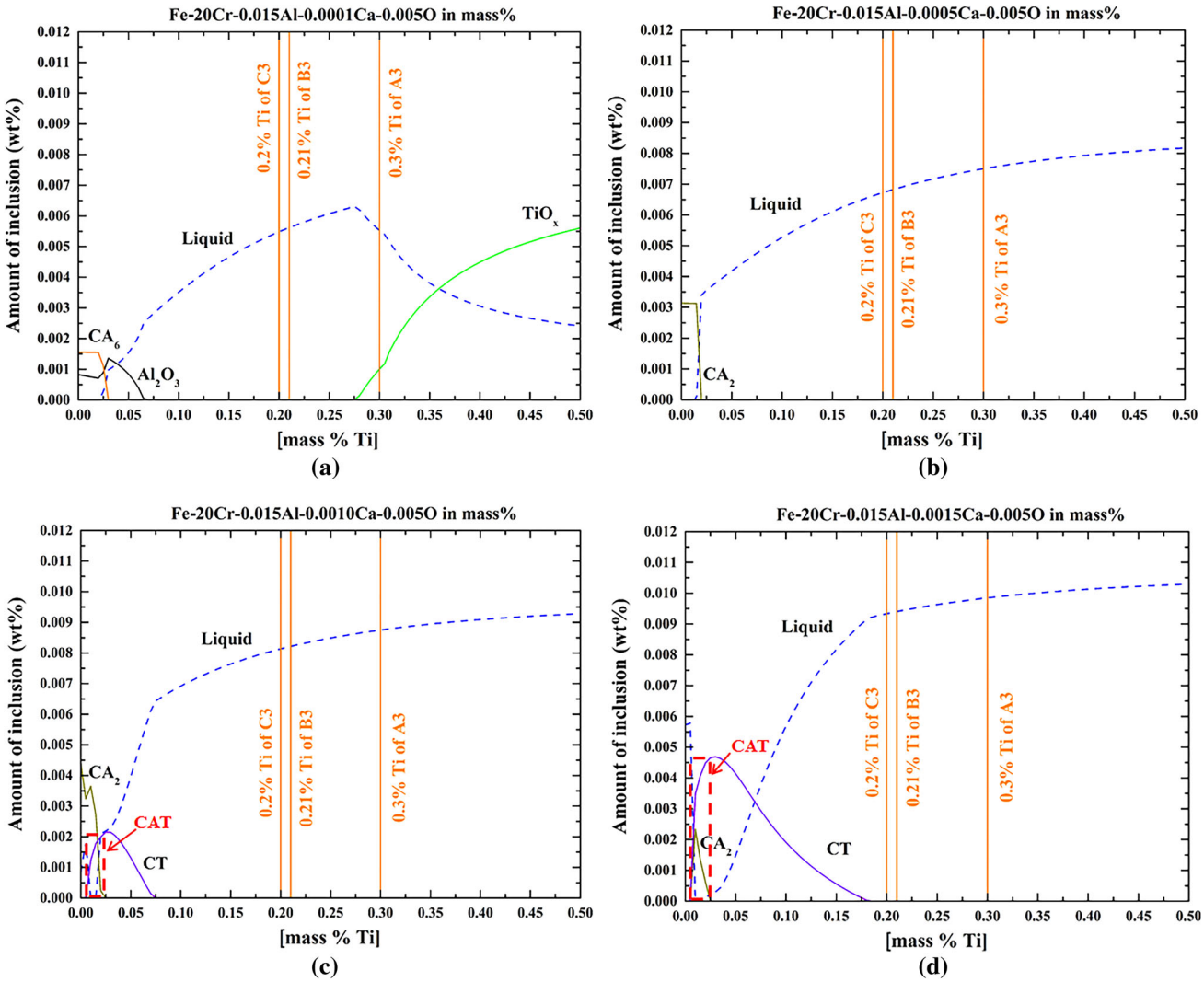

Fig. 10—Equilibrium formation of inclusions during titanium addition process at 1873 K for steel compositions: Fe-20Cr-Ti-0.015Al-0.005O-Ca in mass pct: (*a*) Ca = 1 ppm, (*b*) Ca = 5 ppm, (*c*) Ca = 10 ppm, (*d*) Ca = 15 ppm (CA_2: $CaO{\cdot}2Al_2O_3$, CA_6: $CaO{\cdot}6Al_2O_3$, CT: perovskite ($CaTiO_3$), liquid: liquid oxide, CAT: perovskite ($CaTiO_3$) + CA_2 ($CaO{\cdot}2Al_2O_3$)).

are plotted in Figure 10. It can be found that most of the compositions were located in liquid oxide phase field. However, the compositions of most inclusions in samples A3 and B3 were located out of the liquid oxide phase field, as shown in Figure 5. The metal–inclusion reaction has been experimentally proved to be sufficiently fast,[42] which might lead to the local equilibrium between the molten steel and the inclusions during the titanium addition process. The CAT inclusions consisting of Perovskite ($CaTiO_3$) and CA_2 ($CaO{\cdot}2Al_2O_3$) were firstly formed at the beginning of titanium addition, as marked in Figure 10. Although the CAT inclusions observed in samples would not be formed in molten steel with high titanium content, the local equilibrium in molten steel during titanium addition process could lead to the formation of CAT inclusions in high calcium content steel. The mass percentages of CaO, Al_2O_3, and TiO_x calculated in Figure 10 are marked in the CaO-Al_2O_3-Ti_3O_5 ternary compositional diagram, as shown in Figure 11. It can be seen that the initial calcium content has a significant effect on the evolution of inclusions during titanium addition. When the calcium content was lower than 5 ppm, the inclusion composition would be located in the all liquid oxide phase field with the increase of titanium content in steel. When the calcium content was higher than 10 ppm, solid CAT (perovskite ($CaTiO_3$) + CA_2 ($CaO{\cdot}2Al_2O_3$)) or CT (perovskite ($CaTiO_3$)) inclusions would be formed during the addition of titanium, which might lead to the clogging of the submerged entry nozzle (SEN).[5,19]

C. *Evolution Mechanism of the Oxide Inclusions*

According to the experimental results and thermodynamic calculation, the evolution mechanism of the oxide inclusions during the Ti-bearing stainless steelmaking process is shown schematically in Figure 12. The transformation process can be summarized as the following three steps:

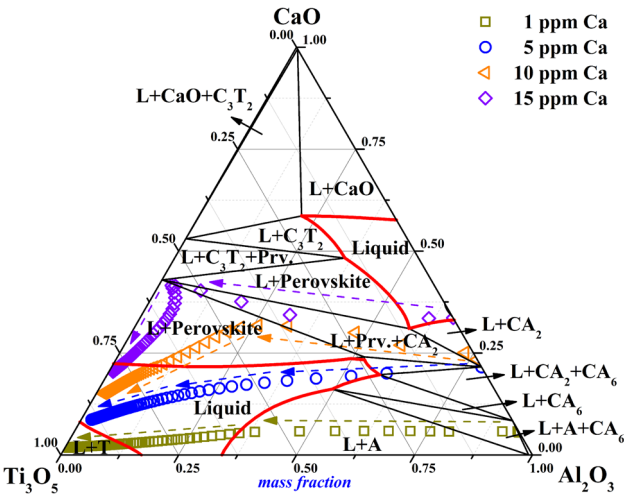

Fig. 11—Composition evolution of inclusions in $CaO-Al_2O_3-Ti_3O_5$ phase diagrams during titanium addition process at 1873 K for steel of composition: Fe-20Cr-Ti-0.015Al-0.005O-Ca in mass pct: Ca = 1 ppm, Ca = 5 ppm, Ca = 10 ppm, Ca = 15 ppm; Ti: 0 to 0.5 wt pct (liquid (L): liquid oxide, CA_2: $CaO{\cdot}2Al_2O_3$, CA_6: $CaO{\cdot}6Al_2O_3$, A: Al_2O_3, perovskite (Prv.): $CaTiO_3$, C_3T_2: $3CaO{\cdot}2TiO_2$, T: Ti_3O_5).

1. After the addition of aluminum at the initial stage of LF refining, the inclusions containing alumina were formed. There was usually several ppm Mg in molten steel due to the $MgO-CrO_x$ refractory. Based on the Al-Mg-O phase diagram, several ppm Mg could easily lead to the formation of $MgO{\cdot}Al_2O_3$ spinel inclusions after Al addition, which also made $MgO{\cdot}Al_2O_3$ inclusions the main inclusions in steel samples. $MgO{\cdot}Al_2O_3$ spinel and alumina inclusions were solid at steelmaking temperature, which could cause the serious clogging of SEN.[10,48,49]
2. In order to remove or modify these unfavorable inclusions, Ca treatment was taken after Al addition. Spherical $CaO-Al_2O_3-MgO$ inclusions were formed after the addition of calcium. According to the morphology and composition of the inclusions, most of $CaO-Al_2O_3-MgO$ inclusions were liquid oxide. Thermodynamic calculation also indicated that several ppm calcium in steel could significantly expand the liquid oxide phase field and decrease the stability of spinel. The formation of these liquid oxide inclusions after calcium treatment can effectively prevent the clogging of SEN.
3. Titanium was added to the molten steel as an alloying element after calcium treatment. The initial calcium

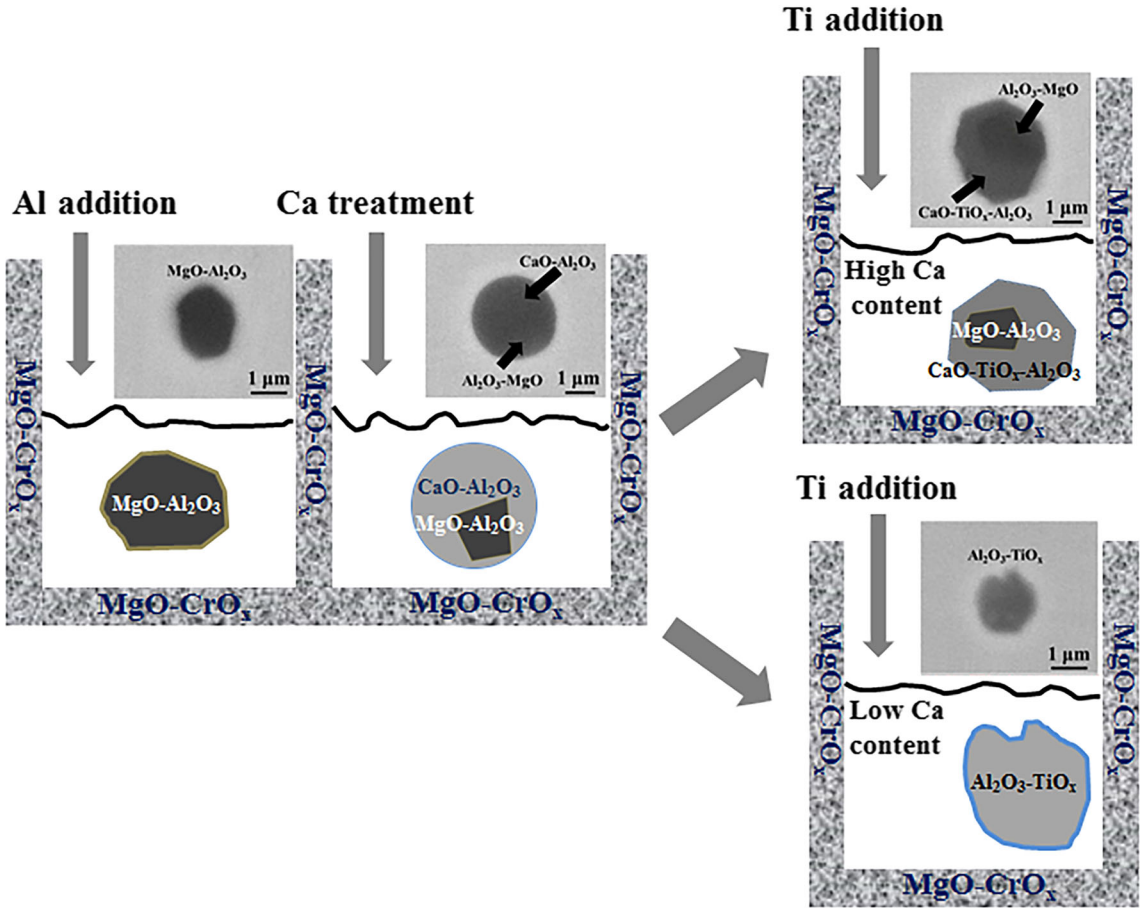

Fig. 12—Schematic illustration of the evolution mechanism of the oxide inclusions in Ti-bearing stainless steel with calcium treatment.

content has an important influence on the evolution of oxide inclusions during titanium addition. When the calcium content was low, it would form liquid Al_2O_3-TiO_x inclusions after Ti addition. When the calcium content was high, inclusions consisting of liquid and $CaTiO_3$ were formed during the titanium addition process. Combined with thermodynamic calculation and experimental results, it can be found that inclusions consisting of liquid and $CaTiO_3$ were formed in molten steel with more than 10 ppm Ca during the Ti addition process. It has been found that inclusions consisting of liquid and $CaTiO_3$ could lead to the clogging of SEN.[5,19]

IV. CONCLUSIONS

In present work, industrial experiments were undertaken to investigate the evolution mechanism of oxide inclusions in Al-killed, Ti-bearing 20Cr stainless steel with Ca treatment. Based on the results of the chemical analysis, inclusion characteristics, and thermodynamic calculation, the following conclusions were obtained:

1. After the addition of Al, the main type of inclusions formed in molten steel was irregular shape $MgO{\cdot}Al_2O_3$ spinel or (Al_2O_3 + spinel) inclusions. Spherical CaO-Al_2O_3-MgO inclusions became the main inclusions after calcium treatment. After titanium addition, two types of inclusions were formed: spherical liquid Al_2O_3-TiO_x-based inclusions and complex CaO-TiO_x-Al_2O_3-MgO inclusions. At the end of LF, the types of inclusions were essentially same as that of after titanium addition.
2. The $MgO{\cdot}Al_2O_3$ spinel inclusions were modified to be spherical CaO-Al_2O_3-MgO inclusions after calcium treatment. Thermodynamic calculation also indicated that several ppm Ca could significantly expand the liquid oxide phase field and decrease the stability of spinel. After titanium addition, most of the compositions of steel were located in or close to the Al_2O_3-TiO_x liquid oxide phase field, which would contribute to reducing the formation of oxide inclusions and increasing the titanium yield.
3. The initial calcium content has a significant effect on the evolution of inclusions during titanium addition process. Liquid Al_2O_3-TiO_x inclusions would be formed after Ti addition in steel with low calcium content. Inclusions consisting of liquid and $CaTiO_3$ were formed in molten steel with more than 10 ppm Ca during the Ti addition process, which could lead to the clogging of SEN. It was necessary to control the calcium content before the addition of titanium.

ACKNOWLEDGMENTS

The authors gratefully express their appreciation to the National Nature Science Foundation of China (Grant No. 51674024), the State Key Laboratory of Advanced Metallurgy at University of Science and Technology Beijing (USTB), and Jiuquan Iron and Steel Co. for supporting this work.

REFERENCES

1. T. Liu, L. Chen, H. Bi, and X. Che: *Acta Metall. Sin.*, 2014, vol. 27, pp. 452–56.
2. J. Cavazos, I. Gomez, and M. Guerrero-Mata: *Mater. Sci. Technol.*, 2011, vol. 27, pp. 530–36.
3. T. Koseki and H. Inoue: *J. Jpn. Inst. Met.*, 2001, vol. 65, pp. 644–51.
4. R. Nunnington and N. Sutcliffe: *Electric Furnace Conf. Proc.*, Phoenix, Arizona. 2001, pp. 1–39.
5. H. Zheng, W. Chen, and Y. Hu: *AISTech Proc.*, 2004, vol. 1, pp. 937–45.
6. S. Basu, S.K. Choudhary, and N.U. Girase: *ISIJ Int.*, 2004, vol. 44, pp. 1653–60.
7. R. Maddalena, R. Rastogi, B. El-Dasher, and A.W. Cramb: *Electric Furnace Conf. Proc.*, ISIS-AIME, 2000, pp. 811–31.
8. S.B. Lee, J.H. Choi, H.G. Lee, P.C.H. Rhee, and S.M. Jung: *Metall. Mater. Trans. B*, 2005, vol. 36B, pp. 414–16.
9. J.J. Pak, J.O. Jo, S.I. Kim, W.Y. Kim, T.I. Chung, S.M. Seo, J.H. Park, and D.S. Kim: *ISIJ Int.*, 2007, vol. 47, pp. 16–24.
10. K. Sakata: *ISIJ Int.*, 2006, vol. 46, pp. 1795–99.
11. J.H. Park and H. Todoroki: *ISIJ Int.*, 2010, vol. 50, pp. 1333–46.
12. H. Goto, K.I. Miyazawa, K.I. Yamaguchi, S. Ogibayashi, and K. Tanaka: *ISIJ Int.*, 1994, vol. 34, pp. 414–19.
13. G. Ye, P. Jönsson, and T. Lund: *ISIJ Int.*, 1996, vol. 36, pp. S105–08.
14. H. Itoh, M. Hino, and S. Ban-Ya: *Metall. Mater. Trans. B*, 1997, vol. 28B, pp. 953–56.
15. J.H. Park, S.B. Lee, and D.S. Kim: *Metall. Mater. Trans. B*, 2005, vol. 36B, pp. 67–73.
16. S. Yang, Q. Wang, L. Zhang, J. Li, and K. Peaslee: *Metall. Mater. Trans. B*, 2012, vol. 43B, pp. 731–50.
17. M. Jiang, X. Wang, B. Chen, and W. Wang: *ISIJ Int.*, 2010, vol. 50, pp. 95–104.
18. Y. Gao and K. Sorimachi: *ISIJ Int.*, 1993, vol. 33, pp. 291–97.
19. G. Qian and G. Cheng: *Conf. of AISTech*, Indianapolis, USA, 2014, vol. 2, pp. 1823-29.
20. H. Matsuura, C. Wang, G. Wen, and S. Sridhar: *ISIJ Int.*, 2007, vol. 47, pp. 1265–74.
21. X. Yin, Y. Sun, Y. Yang, X. Bai, M. Barati, and A. McLean: *Metall. Mater. Trans. B*, 2016, vol. 47B, pp. 3274–84.
22. I.H. Jung, G. Eriksson, P. Wu, and A. Pelton: *ISIJ Int.*, 2009, vol. 49, pp. 1290–97.
23. M.A. Van-Ende, M. Guo, R. Dekkers, M. Burty, J. Van-Dyck, P.T. Jones, B. Blanpain, and P. Wollants: *ISIJ Int.*, 2009, vol. 49, pp. 1133–40.
24. D.C. Park, I.H. Jung, P.C. Rhee, and H.G. Lee: *ISIJ Int.*, 2004, vol. 44, pp. 1669–78.
25. C. Wang, N.T. Nuhfer, and S. Sridhar: *Metall. Mater. Trans. B*, 2009, vol. 40B, pp. 1005–21.
26. C. Wang, N.T. Nuhfer, and S. Sridhar: *Metall. Mater. Trans. B*, 2009, vol. 40B, pp. 1022–34.
27. C. Wang, N.T. Nuhfer, and S. Sridhar: *Metall. Mater. Trans. B*, 2010, vol. 41B, pp. 1084–94.
28. C. Wang, N. Verma, Y. Kwon, W. Tiekink, N. Kikuchi, and S. Sridhar: *ISIJ Int.*, 2011, vol. 51, pp. 375–81.
29. T. Zhang, C. Liu, and M. Jiang: *Metall. Mater. Trans. B*, 2016, vol. 47B, pp. 2253–62.
30. D. Kruger and A. Garbers-Craig: *Metall. Mater. Trans. B*, 2017, vol. 48B, pp. 1514–32.
31. J.W. Kim, S.K. Kim, D.S. Kim, Y.D. Lee, and P.K. Yang: *ISIJ Int.*, 1996, vol. 36, pp. S140–43.
32. C.-W. Seo, S.-H. Kim, S.-K. Jo, M.-O. Suk, and S.-M. Byun: *Metall. Mater. Trans. B*, 2010, vol. 41B, pp. 790–97.
33. L. Zhang and B.G. Thomas: *ISIJ Int.*, 2003, vol. 43, pp. 271–91.
34. J.Z. Li, M. Jiang, X.-F. He, W. Sun, and X.-H. Wang: *Metall. Mater. Trans. B*, 2016, vol. 47B, pp. 2386–99.
35. Y. Ren, L. Zhang, W. Yang, and H. Duan: *Metall. Mater. Trans. B*, 2014, vol. 45B, pp. 2057–71.

36. T. Taniguchi, N. Satoh, Y. Saito, K. Kubota, A. Kumagai, Y. Tamura, and T. Miki: *ISIJ Int*., 2011, vol. 51, pp. 1957–66.
37. E. Zinngrebe, C. Van Hoek, H. Visser, A. Westendorp, and I.-H. Jung: *ISIJ Int*., 2012, vol. 52, pp. 52–61.
38. J.H. Park and D.S. Kim: *Metall. Mater. Trans. B*, 2005, vol. 36B, pp. 495–502.
39. J. Park: *Mater. Sci. Eng. A*, 2008, vol. 472, pp. 43–51.
40. B. Harkness and D. Dyson: *METEC Congr. 94 and 2nd Eur. Continuous Casting Conf*., VDEh, Duesseldorf, Germany, 1994, pp. 70-75.
41. T. Nishi and K. Shimme: *Tetsu-to-Hagané*, 1998, vol. 84, pp. 837–43.
42. G. Okuyama, K. Yamaguchi, S. Takeuchi, and K.-I. Sorimachi: *ISIJ Int*., 2000, vol. 40, pp. 121–28.
43. W.-Y. Cha, T. Miki, Y. Sasaki, and M. Hino: *ISIJ Int*., 2008, vol. 48, pp. 729–38.
44. S.-H. Seok, T. Miki, and M. Hino: *ISIJ Int*., 2011, vol. 51, pp. 566–72.
45. H. Todoroki, F. Kirihara, Y. Kanbe, and Y. Miyazaki: *Tetsu-to-Hagané*, 2014, vol. 100, pp. 539–47.
46. H. Ono, K. Nakajima, S. Agawa, T. Ibuta, R. Maruo, and T. Usui: *Steel Res. Int*., 2015, vol. 86, pp. 241–51.
47. F. Ruby-Meyer: *Scand. J. Metall*., 2000, vol. 29, pp. 206–12.
48. T. Ikemoto and K. Sawano: *Taikabutsu*, 1994, vol. 46, pp. 179–86.
49. S. Ogibayashi: *Taikabutsu*, 1994, vol. 46, pp. 166–74.